OXFORD

Sequence analysis

`RNAscClust`: clustering RNA sequences using structure conservation and graph based motifs

Milad Miladi[1],[†], Alexander Junge[2],[3],[†], Fabrizio Costa[1], Stefan E. Seemann[2],[3], Jakob Hull Havgaard[2],[3], Jan Gorodkin[2],[3],* and Rolf Backofen[1],[2],[4],*

[1]Bioinformatics Group, Department of Computer Science, University of Freiburg, Freiburg im Breisgau, Germany, [2]Center for Non-coding RNA in Technology and Health, University of Copenhagen, Frederiksberg, Denmark, [3]Department of Veterinary and Animal Sciences, University of Copenhagen, Frederiksberg, Denmark and [4]Center for Biological Signalling Studies (BIOSS), Cluster of Excellence, University of Freiburg, Freiburg im Breisgau, Germany

*To whom correspondence should be addressed.

[†]The authors wish it to be known that, in their opinion, the first two authors should be regarded as Joint First Authors.

Associate Editor: Cenk Sahinalp

Abstract

Motivation: Clustering RNA sequences with common secondary structure is an essential step towards studying RNA function. Whereas structural RNA alignment strategies typically identify common structure for orthologous structured RNAs, clustering seeks to group paralogous RNAs based on structural similarities. However, existing approaches for clustering paralogous RNAs, do not take the compensatory base pair changes obtained from structure conservation in orthologous sequences into account.

Results: Here, we present `RNAscClust`, the implementation of a new algorithm to cluster a set of structured RNAs taking their respective structural conservation into account. For a set of multiple structural alignments of RNA sequences, each containing a paralog sequence included in a structural alignment of its orthologs, `RNAscClust` computes minimum free-energy structures for each sequence using conserved base pairs as prior information for the folding. The paralogs are then clustered using a graph kernel-based strategy, which identifies common structural features. We show that the clustering accuracy clearly benefits from an increasing degree of compensatory base pair changes in the alignments.

Availability and Implementation: `RNAscClust` is available at http://www.bioinf.uni-freiburg.de/Software/RNAscClust.

Contact: gorodkin@rth.dk or backofen@informatik.uni-freiburg.de

Supplementary information: Supplementary data are available at *Bioinformatics* online.

1 Introduction

The structure of an RNA molecule or non-coding RNA (ncRNA) is often crucial to its function. A main characteristic is that evolutionary changes in the primary sequence are often compensatory such that, e.g. an A-U base pair in human may correspond to a G-C base pair in mouse, thus preserving a functional RNA structure while (partly) erasing sequence similarity.

In silico genome-wide screens for structured RNAs have therefore focused on finding RNAs with evolutionarily conserved secondary structure (see Backofen and Hess, 2010; Gorodkin *et al.*, 2010; for reviews). A main reason is that it is not feasible to search for structured RNAs on single sequences only, as their secondary structure is not significantly more stable compared to that of random sequences (Rivas and Eddy, 2000). Although all screens take outset in

corresponding or syntenic sequences, two lines of strategies have been employed, one searching for structured RNAs in sequence based alignments and one conducting structural alignments. Whereas the former has the advantage of faster screenings, the latter is able to handle sequence identities below about 60 to 70%. In this identity range sequence based alignments are no longer accurate enough to represent RNA structure conservation (Gardner and Giegerich, 2004; Washietl and Hofacker, 2004). Examples of methods working on sequence based alignments include RNAz (Gruber *et al.*, 2010) and EvoFold (Pedersen *et al.*, 2006). Programs for structural alignment applied to genomic screens includes Foldalign, Dynalign, LocaRNA and CMfinder (Havgaard *et al.*, 2007; Fu *et al.*, 2014; Will *et al.*, 2013a; Yao *et al.*, 2006). Corresponding screens for structure RNAs range from prokaryotes (Uzilov *et al.*, 2006; Weinberg *et al.*, 2010) to fly (Will *et al.*, 2013b) to vertebrates (Smith *et al.*, 2013; Torarinsson *et al.*, 2006, 2008).

The output of each screen for conserved RNA secondary structures is a set of multiple alignments containing orthologous RNAs predicted to adapt a common secondary structure. These sets are largely unannotated and the road to obtain functional evidence for these putative ncRNAs is tedious. One of the most promising annotation strategies would be to detect paralogs in form of RNA families or classes. Whereas members of RNA families originate from a common ancestor, members of an RNA class share the same functional structure without evolutionary relationship (Stadler, 2014). A prominent example for such an RNA class are microRNAs.

An attractive strategy to detect RNA families and classes in computational ncRNA screens is to cluster the RNA candidates based on sequence and structure. Early approaches directly clustered RNA sequences based on their sequence-structure alignment scores (Havgaard *et al.*, 2007; Will *et al.*, 2007), despite the high complexity of at least $O(n^4)$ for aligning two sequences. Albeit recent sequence-structure alignment tools are able to compute the alignment in time quadratic in sequence length (Otto *et al.*, 2014; Will *et al.*, 2015), the overall approach still does not scale to large datasets since it remains quadratic in the number of sequences clustered. For this reason, alignment-free RNA clustering approaches have been introduced (Heyne *et al.*, 2012; Middleton and Kim, 2014).

In this paper, we boost the alignment-free clustering pipeline GraphClust (Heyne *et al.*, 2012) by employing information about covariation contained in the alignments. The GraphClust pipeline works on single sequences and clusters paralogs. Work extending over single sequence clustering has been introduced by EvoFam to cluster EvoFold predictions (Parker *et al.*, 2011). However, these predictions are grounded in sequence based alignments with limited degree of sequence variation. Here, we are interested in uncovering the full potential to search for paralogs including less sequentially conserved structured RNAs that may only be found through the structural alignment strategy. Thus, in contrast to previous work, we here focus on measuring the clustering performance as a function of the degree of compensatory base changes, or equivalently the degree of sequence similarity, in the structural alignments.

We develop RNAscClust, which clusters sequences from an organism of interest that are aligned to their orthologs found in different species. Firstly, RNAscClust represents the sequence stemming from the species of interest in each input alignment as a secondary structure that is obtained by constraining highly conserved base pairs. The pipeline then compares these structures using a graph kernel (Costa and De Grave, 2010). The graph kernel decomposes each structure into several substructures and can be regarded as an extension of k-mer decompositions from sequences to graphs. Comparing these substructures finally induces a similarity measure used to cluster the structures. The usage of locality sensitive hashing techniques (Broder, 1997) enables a complexity linear in the size of the dataset, considerably lower than the quadratic time performance of clustering approaches relying on all-vs-all comparisons.

We compare the performance of RNAscClust to GraphClust using benchmark datasets derived from the Rfam database (Nawrocki *et al.*, 2014). RNAscClust is benchmarked with sets of RNA sequence alignments restricted to specific ranges of sequence identity. Each RNAscClust clustering is compared to a corresponding GraphClust result obtained by clustering human sequences contained in each alignment.

We demonstrate a considerable positive effect of incorporating structure conservation in alignments of orthologous sequences when clustering paralogous RNA sequences from an organism of interest. This results in a beneficial accuracy compared to clustering of single sequences alone, especially for datasets with low to medium sequence identity.

2 Materials and methods

2.1 Clustering approach

This section describes the RNAscClust pipeline and analyzes its computational complexity. RNAscClust accepts a set of multiple alignments as input where each alignment contains a sequence from the organism of interest structurally aligned to its orthologs. Our approach first predicts the secondary structure for the sequence from the organism of interest in each alignment using information about conserved base pairs. The secondary structure is then encoded as a sparse feature vector. Candidate clusters are iteratively selected in linear time and refined in a final post-processing step. Figure 1 compares this structure conservation-aware clustering to single sequence clustering. We furthermore introduce classification and clustering performance measures used in this work.

2.1.1 Representing a multiple sequence alignment as an RNA secondary structure

Let M be the set of structural alignments of RNA sequences to be clustered by RNAscClust. In the first step, we predict the consensus structure S_m of each alignment $m \in M$ to identify conserved base pairs. We chose PETfold (Seemann *et al.*, 2008) in this step as it is shown to perform well for predicting the consensus structure from a set of aligned sequences (Puton *et al.*, 2013). PETfold predicts a consensus structure by taking evolutionary and thermodynamic information into account and assigns a reliability $r \in [0, 1]$ to each base pair. For a given alignment m and reliability threshold τ, a base pair (i, j) is considered conserved if its reliability $r_{ij} \geq \tau$. Conserved base pairs are used as constraints for predicting the secondary structure of the sequence from the species of interest using RNAfold (Lorenz *et al.*, 2011). This allows to project conserved base pairs from the alignments onto the sequence, while tolerating variations in less structurally conserved alignment columns.

Additionally, we use the recently proposed R-scape (Rivas *et al.*, 2016) to identify base pairs with statistically significant (E-value < 0.05) covariation. R-scape assesses the statistical significance of the observed covariation by simulating alignments under the null hypothesis that nucleotide substitutions appear independently in each column under a phylogenetic model. This allows to put further emphasis on covarying base pairs, independent of sequence information, in the clustering process by adding *decorated graphs* (see Section 2.1.2) whenever at least 20% of the base pairs are supported by covariation. The outcome of this first step, illustrated in Figure 2a, is a
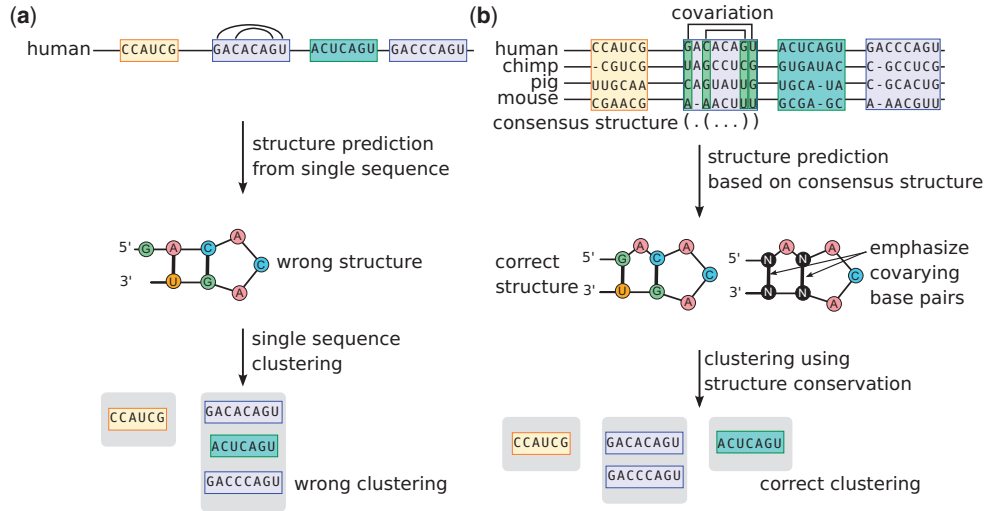
Fig. 1. Hypothetical example to illustrate the difference between single sequence clustering and clustering using conserved structure. Assume the indicated G-U base pair between the first and last nucleotide in the left-most blue human sequence is part of its correct secondary structure. While single sequence structure prediction (**a**) fails to predict the G-U pair, information about covariation contained in the alignment (**b**) yields the correct secondary structure for the human sequence and allows to emphasize covarying base pairs. Taking covariation and conserved structures into account may thus yield an improved clustering
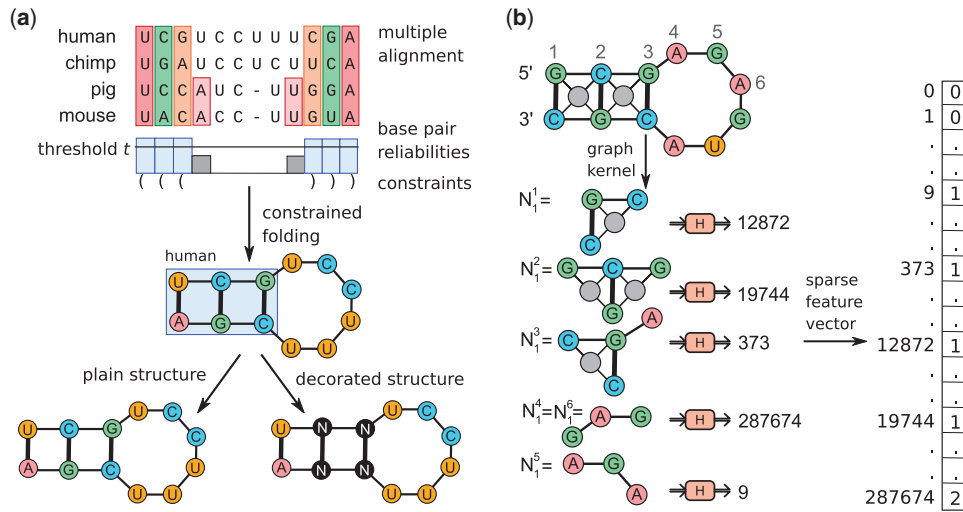

Fig. 2. Representing the constrained folded secondary structure as a graph and feature extraction. (**a**) Base pairs with a reliability greater than t are set as structure constraints (blue boxes) derived from the alignment consensus structure. A constrained secondary structure prediction is performed for the human sequence, the organism of interest in this example. Plain and, if enough covarying base pairs are found, decorated secondary structure are represented as graphs. (**b**) Auxiliary vertices (gray) are added to the secondary structure graph to emphasize stacked base pairs. The secondary structure is decomposed into substructures using a graph kernel. Here, only neighborhood subgraphs for N_1^v and $v = 1, \ldots, 6$ are shown and $d = 0$ which results in the extraction of single root vertices instead of root vertex pairs. The hashing function H encodes each subgraph as an integer which in turn becomes the index of the subgraph in the sparse feature vector counting subgraph occurrences. Since $N_1^4 = N_1^6$, the feature is counted twice while the other neighborhood subgraphs are unique. The feature extraction for N-N decorated structures is implemented the same way

secondary structure representing the alignment m in the remaining part of the RNAscClust pipeline.

2.1.2 Efficient encoding of the RNA secondary structure

RNAscClust follows the approach implemented by Heyne *et al.* (2012) and represents each secondary structure as a graph where nucleotides are encoded as vertices with discrete labels A, C, G, U while the backbone and the base pair relations are encoded as edges. Auxiliary vertices adjacent to four nucleotides forming stacked base pairs are added (see Fig. 2b, top) to emphasize base pair stacks. We define the graph G^m as the secondary structure graph associated with the alignment $m \in M$. Our framework allows to add *path graphs* to G^m to include sequence information.

Path graphs are graphs that only contain the backbone (i.e. the ribose-phosphate bond) as edges. Adding a path graph to G^m allows to consider sequence similarities in addition to similarities at the secondary structure level. Decorated graphs, according to R-scape, are created by representing significantly covarying base pairs as generic N-N pairs. Thus sequence information for these base pairs is removed allowing to match corresponding features between alignments without requiring the exact base pairs to be matched.

In RNAscClust sparse feature vectors are extracted from G^m using the Neighborhood Subgraph Pairwise Distance Kernel (NSPDK) (Costa and De Grave, 2010), a convolutional graph kernel. A graph kernel allows to compute the similarity of two graphs using the dot product in the induced feature space. While graph

kernels commonly define a feature space only implicitly and compute directly the resulting dot product, NSPDK explicitly enumerates the features and stores them in a sparse feature vector that remains of manageable size. More precisely, the NSPDK defines as feature all small subgraph-pairs at short distance from each other as defined in the following.

NSPDK considers neighborhood subgraphs: a neighborhood subgraph $N_r^v(G^m)$ is defined as the subgraph induced by all vertices that are reachable from a given root vertex v in not more than r hops along the edges of G^m. The distance d between a pair of neighborhood subgraphs is defined as the distance between the respective root vertices. Finally, a feature in NSPDK is a pair $N_r^u(G^m)$ and $N_r^v(G^m)$ with root vertices u, v that are at distance d. The complete feature set is generated by considering all possible pairs of neighborhood subgraphs for all values of the parameters r and d such that $r \in \{0, \ldots, r_{max}\}$ and $d \in \{0, \ldots, d_{max}\}$. Each pair of neighborhood subgraphs is then encoded as an integer using a fast hashing procedure (see Fig. 2b; Costa and De Grave, 2010 for details) that yields a low number of hash collisions. One crucial advantage of NSPDK is that given a graph $G = (V, E)$ with vertex set V and edge set E, the size of the associated sparse feature vector (i.e. number of non-zero features) is bounded to a factor of $|V|$, allowing fast computations in subsequent steps. While other graph kernels commonly yield a number of features (i.e. subgraphs) that is exponential in the size of V, NSPDK generates a number of subgraphs that is linear in $|V|$ (Costa and De Grave, 2010).

2.1.3 Similarity notion between RNA alignments

The similarity between two alignments is defined as the dot product of the corresponding sparse feature vectors. As larger values of radius r and distance d tend to generate a larger number of highly specific features, the feature vectors are normalized such that each combination of r and d contributes equally to the final vector encoding. That is, each feature vector $\phi_{r,d}(G)$, generated by neighborhood subgraph pairs of radius r at distance d, is normalized to unit length: $\widehat{\phi}_{r,d}(G) = \phi_{r,d}(G)/||\phi_{r,d}(G)||$ and then assembled into the final feature vector $\phi(G) = \sum_{r \in R, d \in D} \widehat{\phi}_{r,d}(G)$.

2.1.4 Clustering secondary structures

To avoid the quadratic complexity arising from an all-vs-all comparisons of all secondary structures, RNAscClust performs approximate nearest neighbor queries to identify candidate clusters. More precisely, we build an inverse index based on a compact signature (obtained using the min-hash approach (Broder, 1997)) of the feature vectors which can be used to retrieve similar instances with a lookup operation in constant time. See Heyne et al. (2012) for further details. Running the approximate nearest neighbor query on each instance yields candidate clusters each consisting of a set of sequences. All candidate clusters are ranked by their mean pairwise similarity and are accepted or rejected, in rank order, using a greedy procedure. The procedure discards a cluster if it does not contain at least fraction ρ of unseen sequences, i.e. if the candidate cluster overlaps too much with the union of all previously accepted clusters. To further improve the consistency of the retrieved clusters, we post-process each cluster by computing the sequence-structure alignment tree of the clustered sequences using LocARNA (Will et al., 2007, 2012). Sequences belonging to the subtree with the highest average pairwise alignment score are then used to fit a covariance model using Infernal (Nawrocki and Eddy, 2013). The covariance model ultimately decides cluster membership by scanning the entire dataset and populating the cluster with all the instances that score above a bit-score threshold.

2.1.5 Runtime complexity of `RNAscClust`

For the input set of alignments M of size $N = |M|$, let L denote the maximum sequence length in the alignments, let $S = max_{m \in M}(|m|)$ denote an upper bound on the number of sequences per alignment. The initial consensus structure prediction using PETfold and constrained folding using RNAfold have complexity $\mathcal{O}(S \cdot L^3)$ per alignment therefore $\mathcal{O}(N \cdot S \cdot L^3)$ for the complete dataset.

Let m be an alignment with the maximal number of vertices and edges. Generating its encoded graph $G^m = (V_m, E_m)$ has complexity $\mathcal{O}(|V_m| + |E_m|)$ and complexity $\mathcal{O}(N \cdot (|V_m| + |E_m|))$ for the whole dataset. As outlined in Section 2.1.2, generating the sparse feature vectors from G^m has complexity $\mathcal{O}(|V_m|), \mathcal{O}(N \cdot |V_m|)$ for the whole dataset M, by hashing feature vectors to integer codes. Finally, both clustering steps using approximate nearest neighbors queries and post-processing have complexity $\mathcal{O}(N)$ (see Costa and De Grave, 2010; Heyne et al., 2012 for further details). Since in realistic scenarios $N \gg L$ and $N \gg S$, the overall runtime of RNAscClust is $\mathcal{O}(N)$. The runtime of RNAscClust is thus linear in the number of input alignments. Figure 3 depicts the complete RNAscClust pipeline and indicates pipeline steps that are executed in parallel.

2.2 Evaluation metrics

Classification: Consider a binary classification problem. A true positive (TP) is an object correctly classified as positive, a false positive (FP) is an object wrongly classified as positive. Similarly, we define true and false negatives (TN and FN). We use the following measures to assess the performance of a binary classifier:

Precision (also known as positive predictive value) is the fraction of correctly classified positives out of all objects classified as positive, i.e. $TP/(TP + FP)$.

Recall (also known as sensitivity) is the fraction of correctly classified positives out of all positives, i.e. $TP/(TP + FN)$. Finally, *F1-Score* (van Rijsbergen, 1979) is the harmonic mean of Precision and Recall:

$$\text{F1} - \text{Score} = 2 \cdot \frac{\text{Precision} \cdot \text{Recall}}{\text{Precision} + \text{Recall}}$$

In a multi-class scenario, as presented below, the F1-Score is the mean of the class-wise F1-Score weighted by the class size.

Clustering: The *Rand Index* (Rand, 1971) measures the fraction of object pairs that are grouped in the same way in a predicted clustering and the true class assignment. Let a be the number of object pairs that are in the same class and in the same cluster and let b be the number of pairs that are in different classes and in different clusters, then the Rand Index is defined as $(a + b)/(|M| \cdot (|M| - 1)/2)$. The *Adjusted Rand Index* (Hubert and Arabie, 1985), a version of the Rand Index adjusted for chance, is defined as:

$$\text{Adjusted Rand Index} = \frac{\text{Rand Index} - E[\text{Rand Index}]}{1 - E[\text{Rand Index}]}$$

Here, the $E[\text{Rand Index}]$ is the expected Rand Index. The Adjusted Rand Index has an upper bound of 1 and higher values indicate a better agreement between the clustering and the true class assignment.

2.3 Materials

To the best of our knowledge no dataset is available that can be directly used to benchmark RNAscClust. We thus created benchmark datasets following two different approaches to assess the performance of RNAscClust. These benchmarks are named the *Rfam-ome* and *Rfam-cliques* datasets. All benchmark sets were derived from
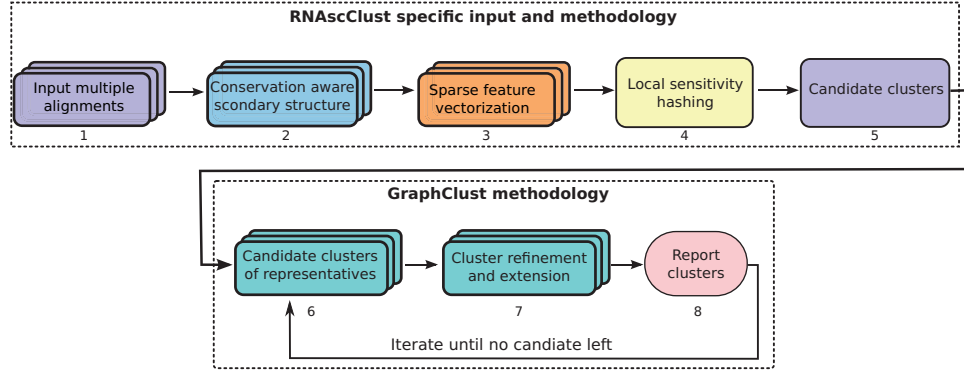
Fig. 3. An overview of `RNAscClust` with steps executed in parallel shown as stacks. The sequence of interest in each alignment is constraint folded to generate a conservation aware secondary structure (steps 1 & 2). The resulting secondary structure graph is transformed into a feature vector in step 3. Using local sensitivity hashing (step 4), candidate clusters are extracted in the fifth step. Then a series of post-processing steps as implemented in `GraphClust` are invoked (steps 6–8): sequences of each cluster are aligned using `LocARNA` and only well aligning sequences are retained. A covariance model is generated with `Infernal` to extend clusters with sequences matching the model. Steps 6–8 are repeated until all candidate clusters are processed

the Rfam database (Nawrocki *et al.*, 2014). The central design idea is to split each Rfam family seed alignment into subalignments and assess how well the clustering pipeline retrieves the Rfam families. Here a subalignment is considered to be a subset of an Rfam seed alignment. Human is the organism of interest in our benchmark. Each subalignment must hence contain a human sequence. The quality of a cluster assignment is measured by rating how well it agrees with the true Rfam family assignment.

2.3.1 Rfam-ome benchmark dataset

The *Rfam-ome* dataset was designed to collect orthologs of a particular human RNA in one subalignment. On the other hand, human paralogs of the same Rfam family are assigned to different subalignments. The *Rfam-ome* benchmark is generated by processing each Rfam family individually. In the first step, human sequences are extracted from the family seed alignment. The genomic locations of these human sequences are then identified by a sequence search against the human genome using `BLAST` (Altschul *et al.*, 1997) while only accepting exact sequence matches. To extend these genomic locations to their genomic neighborhood, context of the same length as the hit is appended in up- and downstream of each hit. Regions syntenic to these extended hits are identified in 26 other species using `LiftOver` (Kent *et al.*, 2003). For each species other than human, exact matches of the organism's sequences contained in the input Rfam seed alignment are searched in the regions orthologous to the human neighborhood. This step yields sequences trusted to be orthologous to the original human sequence hit. Finally a subalignment containing each human (paralog) sequence along with its orthologous sequences is built.

Collecting the subalignments for all Rfam families yields the complete dataset named *Rfam-ome*. Note that all alignments in the *Rfam-ome* benchmark set are created by extracting the respective rows from Rfam seed alignments, while `LiftOver` is solely used to assign orthologous sequences to each human paralog. All genomes as well as chain files used by `LiftOver` were downloaded from the UCSC genome browser (Rosenbloom *et al.*, 2015). Information about the genomes used are listed in the Supplementary Section S1 along with further details about the *Rfam-ome* pipeline.

2.3.2 Rfam-cliques benchmark datasets

The *Rfam-ome* dataset contains only few alignments with mean pairwise sequence identity (PSI) below 70% (Supplementary Section S1.2). Using constraints on the PSI of sequences added to the same

alignment, the *Rfam-cliques* sets control the mean PSI and hence the amount of covariation captured in each alignment.

To generate the *Rfam-cliques* benchmark dataset, each Rfam family seed alignment is processed separately and depicted as a graph. Each sequence in the alignment is a vertex. Two vertices are connected by an edge if they originate from different species. More precisely, for an Rfam family *F* an undirected graph *G* is defined such that

$$G = (V, E),$$

$$V = \{s_i | s_i \text{ is a sequence in the seed alignment of } F\},$$

$$E = \{\{s_i, s_j\} | s_i \text{ and } s_j \text{ belong to different species }\}.$$

We then generate subgraphs of *G* where vertices are connected only if their PSI is in a specific range. For PSI thresholds $l \in [0, 1]$ and $h \in [0, 1]$ such that $l < h$, we define G_l^h, a subgraph of *G*:

$$G_l^h = (V, E_l^h),$$

$$E_l^h = \{\{s_i, s_j\} | \{s_i, s_j\} \in E \text{ and } l < \text{PSI}(s_i, s_j) \leq h\},$$

where $\text{PSI}(s_i, s_j)$ is the PSI of the sequences s_i and s_j. G_l^h contains the same vertices as *G* but only those edges whose corresponding pairs of sequences have a PSI in the range $[l, h]$.

The Algorithm generating the *Rfam-cliques* set for an individual family is outlined below. Subalignments are selected to be maximal cliques with maximum mean PSI in each iteration. A *clique* is a subset of the vertices of a graph in which each pair of vertices is connected by an edge. A clique is *maximal* if it is not a subset of a larger clique. Extracted cliques must have at least five vertices/sequences, one of human origin.

The Algorithm considers different PSI ranges in descending order. It starts with a graph containing vertices in *V* and the edge set $E_{0.9}^{0.95}$. After extracting subalignments as maximal cliques, additional edge sets

$$\Gamma = \{E_{0.8}^{0.9}, E_{0.7}^{0.8}, \dots, E_{0.4}^{0.5}\}$$

are added iteratively to *G* and additional subalignments extracted. This iterative approach extracts cliques with homogeneous similarities first and allows remaining edges to form cliques in subsequent iterations thus yielding a broader PSI distribution in the alignments. Note that Γ contains non-overlapping edge sets selected according to the PSI of the adjacent sequences. The described procedure is performed for each Rfam family separately and the resulting subalignments are combined to create the dataset named *Rfam-cliques High*. Further details about the dataset generation can be found in Supplementary Section S2.

Algorithm generating the *Rfam-cliques* benchmark set for a single family.

1: $G = (V, E) = (V, \varnothing)$
2: $Rfam\text{-}cliques = \varnothing$
3: **for** $(h, l) \in \{(0.95, 0.9), (0.9, 0.8), \ldots, (0.5, 0.4)\}$ **do**
4:     $E = E \cup E_l^h$
5:     **while** G *has a maximal clique of size* ≥ 5 *that contains a human sequence* **do:**
6:         $C = \underset{\substack{c \,\in\, \text{maximal-cliques}(G), \\ c \text{ has human sequence}, \\ \|c\| \geq 5}}{\text{argmax}} \text{meanPSI}(c)$
7:         $Rfam\text{-}cliques = Rfam\text{-}cliques \cup C$
8:         $V = V \backslash C$ ▷ *remove vertices in C from G*
9:     **end while**
10: **end for**
11: **return** *Rfam-cliques*

2.3.3 Rfam-cliques variants

Besides the *Rfam-cliques High* set, we generated two additional variants of the *Rfam-cliques* dataset. The *Rfam-cliques Medium* benchmark set was generated by modifying Line 3 of the Algorithm as follows:

$$(h, l) \in \{(0.8, 0.7), \ldots, (0.5, 0.4)\}$$

The *Rfam-cliques Low* benchmark was generated by setting Line 3 as:

$$(h, l) \in \{(0.7, 0.6), \ldots, (0.5, 0.4)\}$$

This means that each pair of sequences assigned to one subalignment of the *Rfam-cliques Medium* dataset has a PSI of at most 0.80 while each sequence pair contained in a subalignment of the *Rfam-cliques Low* dataset has a PSI of at most 0.70.

Our motivation for creating the *Rfam-cliques Medium* and *Rfam-cliques Low* datasets in addition to the *Rfam-cliques High* benchmark was to test RNAscClust on benchmark sets with varying degrees of mean PSI of the alignments. This in turn allows us to assess the clustering performance of RNAscClust for different amounts of covariation (see Supplementary Section S3.3 for an R-scape covariation analysis). Table 1 lists the mean of the subalignment-wise mean PSI, referred to as *mean PSI* from here on, in each dataset together with the respective number of subalignments and Rfam families. All families comprising less than three alignments were removed from the datasets prior to benchmarking.

2.3.4 Single-sequence datasets

By design, each subalignment in the *Rfam-ome* and *Rfam-cliques* benchmarks contains a human sequence. This enables the comparison of RNAscClust and GraphClust by measuring the degree to which Rfam families are reconstructed using human sequences alone and comparing the outcome to an RNAscClust result harnessing covariance information contained in the structural alignments.

3 Results

3.1 Similarity metric evaluation through classification

First, we assess the quality of the similarity metric, based on dot products of sparse feature vectors, induced by RNAscClust without performing a clustering. An established approach (Videm *et al.*,

Table 1. Benchmark dataset statistics: Mean of the subalignment-wise mean PSI (mean PSI), number of subalignments and Rfam families in the benchmark datasets. Only Rfam families with at least three subalignments are counted

Dataset	Mean PSI	Subalignments	Families
Rfam-ome	0.78	118	28
Rfam-cliques High	0.73	234	48
Rfam-cliques Medium	0.63	166	26
Rfam-cliques Low	0.50	92	10

2014) is to test the performance of a classifier only depending on the pairwise similarities of all objects in the dataset. Here, pairwise similarities based on RNAscClust sparse feature vectors are compared to those similarities generated by GraphClust using a k-Nearest-Neighbor (k-NN) classifier. RNAscClust default parameters are used in all subsequent analyses (RNAscClust's pipeline default values are: $\tau = 0.9$ (see Supplementary Section S3.4), $r_{max} = d_{max} = 3$, $\rho = 50\%$, $\phi = 20$ bits and the size of the feature space is 2^{30}. GraphClust was run with default parameters except that no sequence windowing was performed to obtain a clustering of full-length sequences. Up to 15 rounds of iterative clustering was performed for both tools.).

The evaluation was performed by computing sparse feature vectors for the *Rfam-ome* and *Rfam-cliques* benchmark datasets. The similarity of each pair of alignments was then computed as detailed in Section 2.1.3. A k-Nearest Neighbor classifier combined with 3-fold stratified cross-validation was used to rate the accuracy of the pairwise similarities for the benchmark sets. Stratified cross-validation ensures that each fold contains roughly the same distribution of class labels as the entire dataset. The classifier's parameter k was fixed to 1 and cross-validation was solely used to measure the classification performance. Precision, recall and F1-Score obtained by the k-NN classifier after cross-validation are depicted in Table 2 for $k = 1$. The k-NN classifier based on RNAscClust similarities outperformed the classifier based on GraphClust similarities under all metrics and benchmarks considered. This indicates that the structure conservation-based similarities generated by RNAscClust reflect the Rfam family structure in the *Rfam-ome* and *Rfam-cliques* datasets more accurately than sequence-based similarities produced by GraphClust. We obtained similar results for the 3-NN classifier of both RNAscClust and GraphClust (Supplementary Table S1).

Note that both RNAscClust and GraphClust use sparse feature vectors to iteratively extract clusters from the dataset. These clustering and post-processing steps were not taken into account in the above evaluation and are thus considered next.

3.2 Clustering evaluation

We compared the clustering accuracy of RNAscClust and GraphClust for all benchmark datasets. Both RNAscClust and GraphClust use an iterative clustering procedure, however RNAscClust has the advantage of generating more accurate feature vectors as demonstrated in the previous section. We hence addressed the question to which extent these more accurate feature vectors translate into beneficial clusterings. All RNAscClust and GraphClust clusterings were compared to the Rfam family labels of each benchmark dataset serving as the ground truth clustering. Instances that were not assigned to a cluster by GraphClust or RNAscClust were assigned to singleton clusters.

Figure 4A depicts the Adjusted Rand Index of RNAscClust and GraphClust for the *Rfam-cliques* datasets, Figure 4B shows clustering

Table 2. 1-Nearest-Neighbor classification performance based on pairwise similarities computed by `RNAscClust` and `GraphClust`

Dataset	Precision		Recall		F1-Score	
	RNAscClust	GraphClust	RNAscClust	GraphClust	RNAscClust	GraphClust
Rfam-cliques Low	0.93 ± 0.04	0.79 ± 0.06	0.95 ± 0.01	0.78 ± 0.09	0.93 ± 0.03	0.76 ± 0.09
Rfam-cliques Medium	0.92 ± 0.03	0.83 ± 0.02	0.93 ± 0.01	0.85 ± 0.01	0.92 ± 0.02	0.83 ± 0.02
Rfam-cliques High	0.92 ± 0.01	0.88 ± 0.02	0.91 ± 0.00	0.87 ± 0.00	0.90 ± 0.00	0.86 ± 0.00
Rfam-ome	0.96 ± 0.03	0.88 ± 0.03	0.97 ± 0.02	0.92 ± 0.02	0.96 ± 0.03	0.90 ± 0.03

Mean ± standard deviation of Recall, Precision and F1-Score for 3-fold stratified cross validation are depicted.
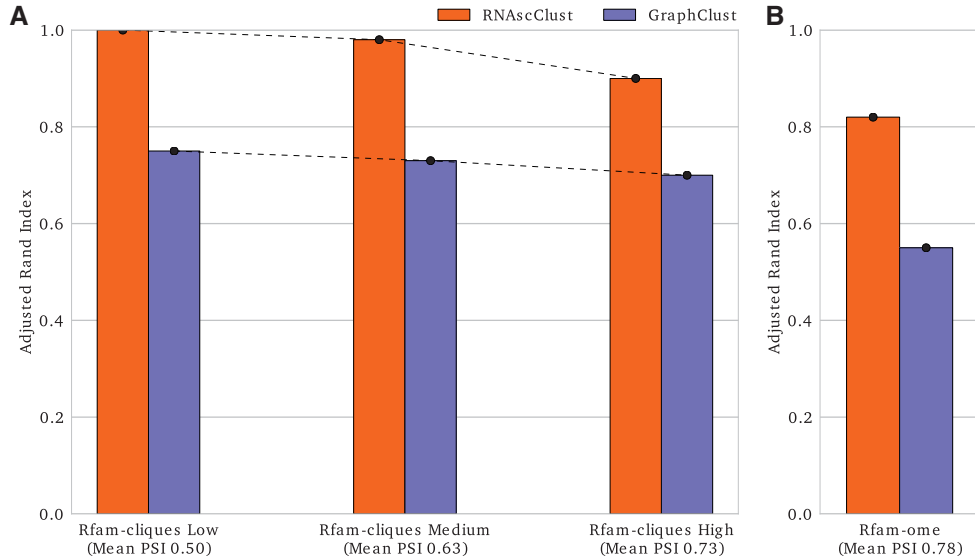

Fig. 4. `RNAscClust` and `GraphClust` clustering performances, measured by the Adjusted Rand Index, depending on the mean of the alignment-wise mean pairwise sequence identity (mean PSI) of the *Rfam-cliques Low*, *Medium* and *High* (**A**) as well as *Rfam-ome* (**B**) benchmark sets

results for *Rfam-ome* set. The Rand Index is depicted in Supplementary Figure S1. Three alternative configurations of the graph encoder are also proposed in Supplementary Section S3 with an overall evaluation depicted in Supplementary Figure S8. These experiments confirmed that `RNAscClust` yields better clustering results than `GraphClust` for all benchmarks. Furthermore, `RNAscClust` performed best for the *Rfam-cliques Low* set while the performance decreased for *Rfam-cliques Medium* and *Rfam-cliques High* sets. Recall that the mean PSI of the *Rfam-cliques Low* dataset is lower than the mean PSI in the *Rfam-cliques Medium* set while the *Rfam-cliques High* has the highest mean PSI. We hypothesize that the performance increase achieved by `RNAscClust` is a result of the larger covariation captured in the *Rfam-cliques Medium* and, even larger, in the *Rfam-cliques Low* set, when compared to the *Rfam-cliques High* set. Additional covariation may yield more accurate structure predictions in each alignment and hence an improved clustering performance.

An example for the largely improved performance of `RNAscClust` compared to `GraphClust` is the SECIS-1 (RF00031) Rfam family in the *Rfam-cliques Medium* set with a mean PSI of 39%. `RNAscClust` correctly clusters all seven human sequences into one cluster consisting only of SECIS-1 sequences; `GraphClust` wrongly places them into multiple clusters mixed with sequences from other families. The same difference is observed in the *Rfam-cliques High* set. For the *Rfam-cliques Low* set, `RNAscClust` outperforms `GraphClust` by, for example, predicting more homogeneous and complete clusters for the well-known structurally conserved tRNA family (RF00005) with a mean PSI of 43%.

4 Discussion

We presented `RNAscClust`, a pipeline for clustering a set of multiple alignments of structured RNAs each containing a sequence from an organism of interest that is aligned to orthologous sequences. `RNAscClust` is geared towards clustering RNA structures by taking structural conservation into account. `RNAscClust` harnesses evolutionarily conserved secondary structure in the clustering process by maintaining conserved base pairs in a constrained folding. This emphasizes the core secondary structure of each alignment while allowing flexibility in the structure arising due to insertions, deletions and non-compensatory mutations. RNA structures are encoded as graphs and a graph kernel is used to generate sparse feature vectors inducing a pairwise similarity notion. `RNAscClust` has a runtime linear in the number of input alignments making it amenable to cluster large datasets.

Employing structure conservation yielded a more accurate pairwise similarity measure and improved the clustering performance. The largest improvements in clustering accuracy were observed for benchmark datasets with low to medium sequence identities. We hypothesize this happens for two reasons: Firstly, evolutionary information contained in the alignments can yield better secondary structure predictions than single sequence folding, explaining the increased clustering performance. Secondly, since `RNAscClust` focuses on evolutionarily conserved base pairs when comparing secondary structures between alignments, identifying these conserved base pairs enables a better estimation of the ncRNA transcript boundaries within the alignment. This helps further improving the secondary structure prediction accuracy in comparison with single sequence clustering.

RNAscClust could be extended by an improved post-processing step. For instance, a novel post-processing step based on CMcompare (Höner zu Siederdissen and Hofacker, 2010) could be used to improve the clustering performance. The approach would be based on covariance models trained for each alignment which are afterwards compared using the Link score as computed by CMcompare. The graph kernel could be extended to allow for vectors of real numbers as node and edge labels. This way, both nucleotide and base pair distributions in the input alignments could be encoded after defining an appropriate similarity function for subgraphs.

RNAscClust produces accurate clusterings while running in linear time. This will facilitate the interpretation of currently available and future large scale genomic screens for structured RNAs potentially containing millions of instances to be clustered (e.g. Smith *et al.*, 2013).

Pipeline availability: RNAscClust is available as source code and as a Docker container (Merkel, 2014) making it possible to run the pipeline without the need to install individual dependencies. Furthermore the container allows to reproduce all Figures and Tables shown in Section 3.

References

Altschul,S.F. *et al.* (1997) Gapped BLAST and PSI-BLAST: a new generation of protein database search programs. *Nucleic Acids Res.*, **25**, 3389–3402.

Backofen,R. and Hess,W.R. (2010) Computational prediction of sRNAs and their targets in bacteria. *RNA Biol.*, **7**, 33–42.

Broder,A.Z. (1997). On the resemblance and containment of documents. In: *Compression and Complexity of Sequences 1997 (Proceedings)*, pp. 21–29.

Costa,F. and De Grave,K. (2010). Fast neighborhood subgraph pairwise distance kernel. In: *Proceedings of the 27th International Conference on Machine Learning (ICML-10), Haifa, Israel*, pp. 255–262. Omnipress.

Fu,Y. *et al.* (2014) Dynalign II: common secondary structure prediction for RNA homologs with domain insertions. *Nucleic Acids Res.*, **42**, 13939–13948.

Gardner,P.P. and Giegerich,R. (2004) A comprehensive comparison of comparative RNA structure prediction approaches. *BMC Bioinformatics*, **5**, 18.

Gorodkin,J. *et al.* (2010) De novo prediction of structured RNAs from genomic sequences. *Trends Biotechnol.*, **28**, 9–19.

Gruber,A.R. *et al.* (2010). RNAz 2.0: Impoved noncoding RNA detection. In: *Proceedings of the Pacific Symposium on Biocomputing 2010*, pp. 69–79.

Havgaard,J.H. *et al.* (2007) Fast pairwise structural RNA alignments by pruning of the dynamical programming matrix. *PLoS Comput. Biol.*, **3**, 1896–1908.

Heyne,S. *et al.* (2012) GraphClust: alignment-free structural clustering of local RNA secondary structures. *Bioinformatics*, **28**, i224–i232.

Höner zu Siederdissen,C. and Hofacker,I.L. (2010) Discriminatory power of RNA family models. *Bioinformatics*, **26**, i453–i459.

Hubert,L. and Arabie,P. (1985) Comparing partitions. *J. Class.*, **2**, 193–218.

Kent,W.J. *et al.* (2003) Evolution's cauldron: Duplication, deletion, and rearrangement in the mouse and human genomes. *Proc. Natl. Acad. Sci. U. S. A.*, **100**, 11484–11489.

Lorenz,R. *et al.* (2011) ViennaRNA package 2.0. *Algorithms Mol. Biol.*, **6**, 1–14.

Merkel,D. (2014) Docker: lightweight linux containers for consistent development and deployment. *Linux J.*, **2014**, 2.

Middleton,S.A. and Kim,J. (2014) NoFold: RNA structure clustering without folding or alignment. *RNA*, **20**, 1671–1683.

Nawrocki,E.P. and Eddy,S.R. (2013) Infernal 1.1: 100-fold faster RNA homology searches. *Bioinformatics*, **29**, 2933–2935.

Nawrocki,E.P. *et al.* (2014) Rfam 12.0: updates to the RNA families database. *Nucleic Acids Res.*, **43**, D130–D137.

Otto,C. *et al.* (2014) ExpaRNA-P: simultaneous exact pattern matching and folding of RNAs. *BMC Bioinformatics*, **15**, 6602.

Parker,B.J. *et al.* (2011) New families of human regulatory RNA structures identified by comparative analysis of vertebrate genomes. *Genome Res.*, **21**, 1929–1943.

Pedersen,J.S. *et al.* (2006) Identification and classification of conserved RNA secondary structures in the human genome. *PLoS Comput. Biol.*, **2**, e33.

Puton,T. *et al.* (2013) CompaRNA: a server for continuous benchmarking of automated methods for RNA secondary structure prediction. *Nucleic Acids Res*, **41**, 4307.

Rand,W.M. (1971) Objective criteria for the evaluation of clustering methods. *J. Am. Stat. Assoc.*, **66**, 846–850.

Rivas,E. and Eddy,S.R. (2000) Secondary structure alone is generally not statistically significant for the detection of noncoding RNAs. *Bioinformatics*, **16**, 583–605.

Rivas,E. *et al.* (2016) A statistical test for conserved RNA structure shows lack of evidence for structure in lncRNAs. *Nat. Methods*.

Rosenbloom,K.R. *et al.* (2015) The UCSC Genome Browser database: 2015 update. *Nucleic Acids Res.*, **43**, D670–D681.

Seemann,S.E. *et al.* (2008) Unifying evolutionary and thermodynamic information for RNA folding of multiple alignments. *Nucleic Acids Res.*, **36**, 6355–6362.

Smith,M.A. *et al.* (2013) Widespread purifying selection on RNA structure in mammals. *Nucleic Acids Res.*, **41**, 8220–8236.

Stadler,P.F. (2014) Class-specific prediction of ncRNAs. *Methods Mol. Biol.*, **1097**, 199–213.

Torarinsson,E. *et al.* (2006) Thousands of corresponding human and mouse genomic regions unalignable in primary sequence contain common RNA structure. *Genome Res.*, **16**, 885–889.

Torarinsson,E. *et al.* (2008) Comparative genomics beyond sequence-based alignments: RNA structures in the ENCODE regions. *Genome Res.*, **18**, 242–251.

Uzilov,A.V. *et al.* (2006) Detection of non-coding RNAs on the basis of predicted secondary structure formation free energy change. *BMC Bioinformatics*, **7**, 173.

van Rijsbergen,C.J. (1979). *Information Retrieval*. 2nd edn. Butterworth, London.

Videm,P. *et al.* (2014) BlockClust: efficient clustering and classification of noncoding RNAs from short read RNA-seq profiles. *Bioinformatics*, **30**, i274–i282.

Washietl,S. and Hofacker,I.L. (2004) Consensus folding of aligned sequences as a new measure for the detection of functional RNAs by comparative genomics. *J. Mol. Biol.*, **342**, 19–30.

Weinberg,Z. *et al.* (2010) Comparative genomics reveals 104 candidate structured RNAs from bacteria, archaea, and their metagenomes. *Genome Biol.*, **11**, R31.

Will,S. *et al.* (2007) Inferring non-coding RNA families and classes by means of genome-scale structure-based clustering. *PLoS Comput Biol.*, **3**, e65.

Will,S. *et al.* (2012) LocARNA-P: Accurate boundary prediction and improved detection of structural RNAs. *RNA*. **18**, 900–914.

Will,S. *et al.* (2013a) LocARNAscan: Incorporating thermodynamic stability in sequence and structure-based RNA homology search. *Algorithms Mol. Biol.*, **8**, 14.

Will,S. *et al.* (2013b) Structure-based whole-genome realignment reveals many novel noncoding RNAs. *Genome Res.*, **23**, 1018–1027.

Will,S. *et al.* (2015) SPARSE: quadratic time simultaneous alignment and folding of RNAs without sequence-based heuristics. *Bioinformatics*, **31**, 2489–2496.

Yao,Z. *et al.* (2006) CMfinder–a covariance model based RNA motif finding algorithm. *Bioinformatics*, **22**, 445–452.